Pharm Res (2011) 28:41–57
DOI 10.1007/s11095-010-0169-8

RESEARCH PAPER

Design, Optimization and Characterisation of Polymeric Microneedle Arrays Prepared by a Novel Laser-Based Micromoulding Technique

Ryan F. Donnelly • Rita Majithiya • Thakur Raghu Raj Singh • Desmond I. J. Morrow • Martin J. Garland • Yusuf K. Demir • Katarzyna Migalska • Elizabeth Ryan • David Gillen • Christopher J. Scott • A. David Woolfson

Received: 29 November 2009 / Accepted: 4 May 2010 / Published online: 19 May 2010
© Springer Science+Business Media, LLC 2010

ABSTRACT

Purpose Design and evaluation of a novel laser-based method for micromoulding of microneedle arrays from polymeric materials under ambient conditions. The aim of this study was to optimise polymeric composition and assess the performance of microneedle devices that possess different geometries.

Methods A range of microneedle geometries was engineered into silicone micromoulds, and their physicochemical features were subsequently characterised.

Results Microneedles micromoulded from 20% w/w aqueous blends of the mucoadhesive copolymer Gantrez® AN-139 were surprisingly found to possess superior physical strength than those produced from commonly used pharma polymers. Gantrez® AN-139 microneedles, 600 μm and 900 μm in height, penetrated neonatal porcine skin with low application forces (>0.03 N per microneedle). When theophylline was loaded into 600 μm microneedles, 83% of the incorporated drug was delivered across neonatal porcine skin over 24 h. Optical coherence tomography (OCT) showed that drug-free 600 μm Gantrez® AN-139 microneedles punctured the *stratum corneum* barrier of human skin *in vivo* and extended approximately 460 μm into the skin. However, the entirety of the microneedle lengths was not inserted.

Conclusion In this study, we have shown that a novel laser engineering method can be used in micromoulding of polymeric microneedle arrays. We are currently carrying out an extensive OCT-informed study investigating the influence of microneedle array geometry on skin penetration depth, with a view to enhanced transdermal drug delivery from optimised laser-engineered Gantrez® AN-139 microneedles.

KEY WORDS laser engineering · microneedles · optical coherence tomography · transdermal drug delivery

R. F. Donnelly (✉) · R. Majithiya · T. R. R. Singh · D. I. J. Morrow · M. J. Garland · Y. K. Demir · K. Migalska · E. Ryan · C. J. Scott · A. D. Woolfson
School of Pharmacy, Queen's University Belfast
Medical Biology Centre
97 Lisburn Road
Belfast BT9 7BL, UK
e-mail: r.donnelly@qub.ac.uk

D. Gillen
Blue Acre Technology
Aiken Business Park, Old Coe's Road
Dundalk, County Louth, Ireland

INTRODUCTION

Microneedle arrays are minimally invasive devices that can be used to by-pass the *stratum corneum* barrier and thus achieve enhanced transdermal drug delivery. Microneedles (MN) (50–900 μm in height, up to 100 MN cm^{-2}) with diverse geometries have been produced from silicon, metal, carbohydrates and polymers using various microfabrication techniques (1,2). MN have been prepared using chemical isotropic etching, injection moulding, reactive ion etching, surface/bulk micromachining, micromoulding and lithography-electroforming-replication (3–8).

MN are applied to the skin surface and pierce the epidermis (devoid of nociceptors), creating microscopic holes through which drugs diffuse to the dermal microcirculation. MN can be made long enough to penetrate to the dermis, but are typically short and narrow enough to avoid stimulation of dermal nerves. Solid MN can be used to puncture skin before or after application of a drug-loaded

patch or can be pre-coated with drug prior to insertion. Biodegradable/water soluble solid MN break down/dissolve in skin to release incorporated drug. Hollow bore MN allow diffusion or pressure-driven flow of drugs through a central lumen.

A particular advantage of MN technology is that drug substances with high molecular weights and/or very water-soluble drugs can be efficiently delivered transdermally (1,2). The rate of drug delivery can now be almost exclusively controlled by the drug delivery system, rather than the *stratum corneum*. MN have been shown to enhance transdermal delivery of a wide range of molecules, including aminolevulinic acid (9), anthrax vaccine (10), β-galactosidase (11), calcein (12), bovine serum albumin (13), desmospressin (14), erythropoietin (15), meso-tetra (N-methyl-4-pyridyl)porphine tetra tosylate (16), ovalbumin (17) and plasmid DNA (10,11). The most widely studied drug with regards to MN-mediated delivery is insulin, with enhanced skin permeation reported *in vitro* (12,18) and *in vivo* (12,19).

MN arrays do not cause pain on application (20), and initial evidence has recently shown that the risk of development of skin infection is minimal (21). Indeed, no reports of MN-associated skin infection have been published to date. However, their use is associated with a number of problems: silicon is not an FDA-approved biomaterial, and broken silicon or metal MN could cause skin problems (2); clean room processing can significantly increase costs (22); solid, non-coated needles require a two-step application process, which is undesirable (2); accurately coating MN is difficult, and these only deliver a very small amount (<1 mg) of drug as a bolus only (2); hollow MN have only one outlet and can become blocked by compressed dermal tissue (23). Heating of polymers or carbohydrates when moulding microneedles can cause drug breakdown (24,25). In addition, various research group have reported that the microchannels created by MN array application tend to close within 2 h under non-occluded conditions (26,27).

Recently, Lee *et al.* (28) described micromoulded MN arrays prepared from aqueous gels of water-soluble polymers under ambient conditions. Our own work to date has involved the use of silicon MN arrays prepared by KOH-based wet-etching (9,16,21) and micromoulding of carbohydrate microneedles using these silicon arrays as master templates (25). We have found the wet-etch process to be limited in terms of the MN height and spacing achievable and found carbohydrate materials difficult to process. In the present study, we describe a novel excimer laser-based method for micromoulding of microneedle arrays prepared from polymeric materials under ambient conditions and aim to optimise MN geometry and polymeric composition. We also describe the utility of optical coherence tomography in studying MN insertion depth and position in human skin *in vivo*.

MATERIALS AND METHODS

Chemicals

Gantrez® AN-139, a copolymer of methylvinylether and maleic anhydride (PMVE/MA) was provided by ISP Co. Ltd., Guildford, UK. Theophylline, poly (vinyl) alcohol (98–99% hydrolysed) (PVA), alginic acid and galactose were obtained from Sigma Aldrich, Dorset, UK. Carbopol® 971 P-NF was obtained from Surfachem Group Ltd., Leeds, UK. Silastic® 9280/60E silicone elastomer was obtained from Dow Corning, Wiesbaden, Germany. All other chemicals used were of analytical reagent grade.

Fabrication of Laser-Engineered Silicone MN Moulds

Laser-engineered silicone micromould templates were prepared on the surface of 1.0-mm-thick silicone sheets. Briefly, silicone elastomer (LSR9-9508-30, Polymer Systems Technology, Wycombe, UK) was poured into a custom-made aluminium mould and cured overnight at 40°C. A laser-machine tool (BluLase® Micromachning System, Blueacre Technology, Dundalk, Ireland) with a laser (Coherent Avia, Coherent Inc., Pittsburgh, USA) emitting a beam having a wavelength of 355 nm and a pulse length of 30 ns, which is variable from 1–100 kHz, was then employed. The maximum average power of the laser was 7 W, giving deliverable pulse energy of 175 uJ. The energy distribution of the beam was Gaussian shaped, with a M^2 value <1.2. The M^2 factor is a standard measure of laser beam quality. A diffraction-limited beam has an M^2 factor of 1 and is a Gaussian beam. Smaller values of M^2 are physically not possible. The M^2 factor of a laser beam limits the degree to which the beam can be focused. Accordingly, the smaller the M^2 value, the smaller the focal spot and the more efficient the processing. M^2 values less than 1.5 are desirable for laser micromachining applications. The laser was controlled by BluLase® LasControl® computer software (Blueacre Technology, Dundalk, Ireland), which allows the operator full control of the laser power and repetition rates, as well as controlling the stages by G-Code (functions in the numerical control programming language). An illustration of the system set-up is shown in Fig. 1. The laser beam was directed by a sequence of three mirrors through an aperture and into a galvanometer (Scanlab hurryScan® 10, SCANLAB Inc., Munich, Germany), which is driven by a computer interface board (Scanlab RTC4 card, SCANLAB Inc., Munich, Germany). The galvanometer allows a laser beam to be positioned

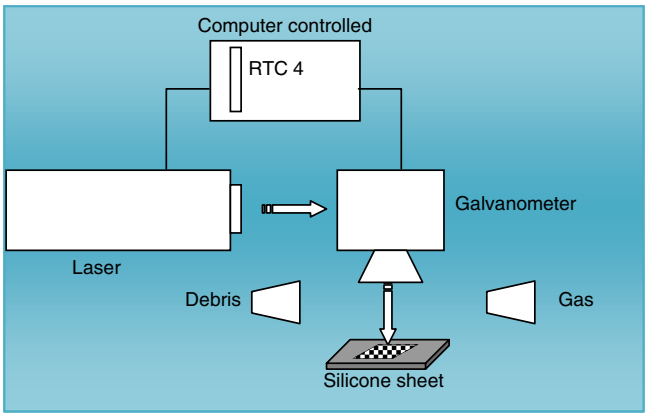

Fig. 1 Illustration of setup of the laser engineering process.

within a field of view of 40 mm×40 mm. The Scanlab RTC4 card is a computer interface board, which provides synchronous, interference-resistant control of scan systems and lasers in real time.

The galvanometer can be controlled by either importing a CAD (computer-aided design) file directly onto the control computer, or the system directly through the graphical user interface. The use of a CAD-controlled galvanometer negates the need for the type of masks used in excimer-based projection laser patterning. The material to be processed (silicone sheet) is placed on the stage (under the galvanometer) and held stationary by a vacuum chuck while being machined. To remove any debris, an air assist was used to blow ablated material into an extraction unit. The laser beam was focused to a spot size of 14.0 μm and scanned at a speed of 4,000 mm/s over the surface of the silicone sheet in the pattern determined by the CAD file. A major advantage of the laser drilling process is that needle height and density are not restricted by the manufacturing process itself. Through a process of 2.5 D laser milling, MN moulds with a varied base diameter, height and interspacing can be produced.

Silicone elastomer micromoulds were prepared using custom-made aluminium containers with fitted aluminium stubs in the centre. The silicone elastomer was carefully poured into the aluminium container so that the level of the silicone was approximately 5 mm above the surface of the aluminium stubs. To eliminate entrapped air, the containers were centrifuged for 15 min at 3,500 rpm before curing overnight at 40.0°C. The silicone elastomer mould was then removed from the aluminium container by gently pressing a metal rod against an opening in the base of the device. The laser-engineered micromould templates were cut in dimensions to exactly fit the silicone mould. The templates were then glued into the mould using silicone elastomer, which was cured at 40°C for 40 min (Fig. 2). In order to clean the prepared moulds, they were sonicated in warm water for 30 min. This process could be used to produce MN arrays possessing different geometries (Fig. 3), where all parameters are variable.

Fabrication of Water-Soluble Polymeric MN

The following polymeric materials were used to prepare corresponding 3×3 MN arrays (dimensions 600 μm in height, 300 μm in width, and an interspacing of 300 μm): PVA, alginic acid, Carbopol® 971 and Gantrez® AN-139. A 30% w/w aqueous solution of PVA was prepared by adding the required mass of PVA to deionised water, followed by heating at 80.0°C for 4.0 h, until a clear gel was formed. Upon cooling, the blend was then readjusted to the final concentration of 30% w/w by addition of an appropriate amount of deionised water. A 10% w/w aqueous solution of alginic acid was prepared by adding the required mass of alginic acid to deionised water, followed by heating at 70°C for 30 min and readjusting to the final concentration of 10%w/w with deionised water. A 10% w/v aqueous Carbopol® 971-P NF blend was prepared by adding the required amount of polymer to distilled water with constant stirring at 800.0 rpm. Once a homogenous gel was formed, it was neutralised using 10 M NaOH to pH6, thus increasing the viscosity of the gel. A 20% w/w aqueous solution of Gantrez® AN-139 was prepared by adding the required mass of Gantrez® AN-139 to ice-cold deionised water, followed by vigorous stirring and heating at 95°C until a clear gel was obtained, due to hydrolysis of the anhydride form of the copolymer to the corresponding acid. Upon cooling, the blend was then readjusted to the final concentration of 20% w/w by addition of an appropriate amount of deionised water. In each case, the resultant solutions were then poured into the silicone micromoulds, centrifuged for 15 min at 3,500 rpm, and allowed to dry under ambient conditions for 24 h.

Measurement of MN Compression Force

The effect of applying a known axial compression load (i.e., force applied parallel to the MN vertical axis) to the prepared polymeric MN was assessed using a TA.XT-plus Texture Analyser (Stable Micro Systems, Surrey, UK). MN arrays were visualised before and after application of the compression load using a light microscope (GXMGE-5 digital microscope, Laboratory Analysis Ltd., Devon, UK). MN arrays were attached to the moveable cylindrical probe (length 5 cm, cross-sectional area 1.5 cm^2) of the Texture Analyser using double-sided adhesive tape. The test station pressed MN arrays against a flat block of aluminium of dimensions 9.2×5.2 cm at a rate 0.5 mm/s for 30 s and a force of 0.36 N per needle. Pre-test and post-test speeds were 1 mm/s, and the trigger force was set at 0.049 N. The height of each MN was measured after testing using the

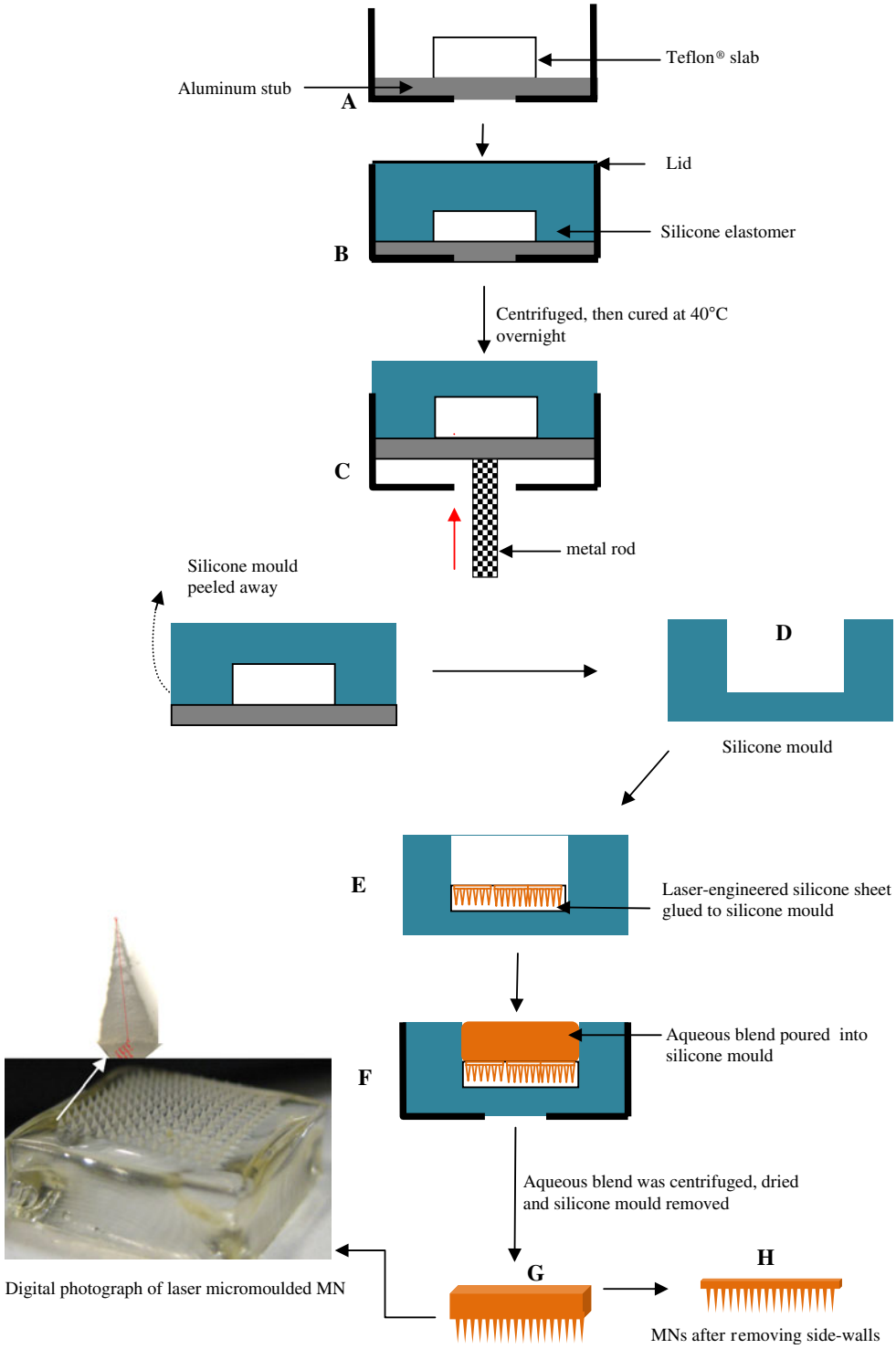

Fig. 2 Diagrammatic representation of the steps involved in preparation of laser-engineered MN arrays. A Teflon® slab is attached to an aluminium stub using cyanoacrylate glue (**A**). Silicone is added to the mould and centrifuged at 3,500 rpm for 15 min (**B**). After curing overnight, the contents of the aluminium container are removed by pressing a metal rod against the aluminium stub (**C**). Silicone mould is carefully peeled away from the aluminium stub (**D**). A laser-engineered silicone sheet is attached to the bottom of the silicone mould using cyanoacrylate adhesive (**E**). Aqueous polymer gel is transferred to the silicone mould (**F**). The mould is centrifuged, and upon hardening, the silicone mould is carefully peeled away from the MN array (**G**). Side-walls of MN arrays were cut-off by means of a hot scalpel blade (**H**).

ruler function of the microscope software so that the percentage change in MN height could be calculated.

Measurement of MN Insertion Force into Excised Neonatal Porcine Skin

The force required to insert polymeric MN into excised porcine epidermis was determined using the Texture Analyser. Neonate porcine skin, a good model for human skin in terms of hair sparseness and physical properties (29,30), was obtained from stillborn piglets and immediately (<24.0 h after birth) excised and trimmed to a thickness of 400 μm using an electric dermatome (Integra Life Sciences™, Padgett Instruments, NJ, USA). Skin was then stored in aluminium foil at −20°C until further use. Using double-sided adhesive tape, MN arrays were carefully attached to

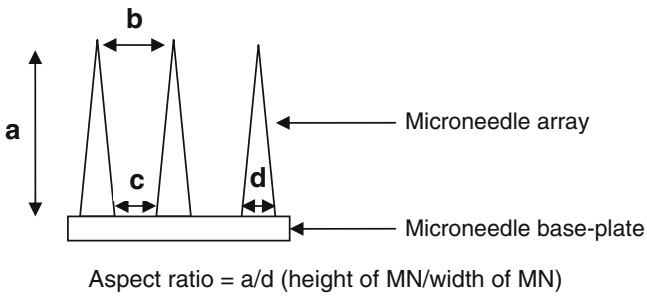

Fig. 3 Diagrammatic representation of a microneedle array and its geometrical parameters: (**a**) height of MNs in array (**b**) interspacing of MN tips (**c**) interspacing of MN bases (**d**) width of MN at base.

the moveable cylindrical probe. The *stratum corneum* surface of the skin was dried with tissue paper, and the skin was placed, dermis side down, on a 500-μm-thick sheet of dental wax, and this assembly was then secured on a wooden block for support. The probe was lowered onto the skin at a speed of 0.5 mm s^{-1} until the required force was exerted. Forces were held for 30 s and varied from 0.0056 N to 0.44 N per needle (obtained by dividing the applied force by the number of MN in an array). Once the target force was reached, the probe was moved upwards at a speed of 0.5 mm s^{-1}. After removal of MN arrays, methylene blue solution (1,000 μg ml^{-1}) was applied to the upper surface of the epidermis for 20 min so holes could be visualised. Excess solution was gently wiped off from the skin surface with dry tissue paper and then with normal saline solution. Subsequently, skin was viewed under the digital microscope. The number of visible holes created by MN arrays was counted so that correlation between applied force and the percentage of percutaneous penetration (number of holes observed/number of holes expected ×100) could be determined.

Measurement of Base-Plate Break Strength and Flexibility

The break strength and degree of flexibility of MN base-plates (polymeric plate upon which MN are formed) were assessed using the Texture Analyser. Base-plates were prepared in the same way as MN arrays, but instead using moulds with no MN holes. MN base-plates of 10×10 mm were placed on two aluminium blocks, which were previously fixed on the working stage of the Texture Analyzer, as shown in Fig. 4. For all measurements, the Texture Analyser was set in compression mode, and a cuboidal aluminium probe (5.5 cm in length) with a blunt end (1.0 mm thickness) was moved towards the MN base-plates at a speed of 2 mm s^{-1} with a maximum distance of travel of 5 mm. Only results from MN base-plates that were observed to break in the middle region during testing were retained. From the peak maximum of the force-distance curve, the break strength of the base-plates was calculated. Equation 1 was used to determine the degree of flexibility of the MN base-plates, as embodied by the angle of base-plate bending upon break, θ, and is explained in detail in Fig. 4.

$$\mathbf{tan}\,\theta = \frac{y}{x} = \frac{Opposite}{adjacent} \qquad Therefore, \quad \mathbf{tan}\,\theta = \frac{b}{a/2} \qquad (1)$$

where a is the initial length of the MN base-plate, b is the distance travelled by the probe before the MN base-plate was broken and θ is the angle determined at the point when the base-plate was broken. All tests were carried out at ambient conditions of 22±2°C and a relative humidity of 43±2% (Hygrometer Testo 608-H1, Testo, Ltd., Hampshire, UK).

Transverse Failure Force of MN Arrays

The transverse failure forces of MN arrays (3×3) were measured with the Texture Analyser again in compression mode. A compound table for a micro drill device (Axminster Power Tool Centre Ltd., Axminster, Devon, UK), consisting of four T slots used for clamping the MN, and equipped with a fine adjustment wheel on the front and left side, as shown in Fig. 5, was employed. A specially designed aluminium probe (3.7 mm thickness at the tip) (Fig. 5) was moved towards the MN arrays at a speed of 0.05 mm s^{-1}. The position of the MN array was fine-adjusted so that the probe fractured the MNs at known height. From the peak maximum of the force-distance curve for each row of MNs (3 in each row) in an array, the force required to fracture a single MN was determined by dividing by 3. All MN of each array were visually examined using a digital microscope before and after fracture testing and changes in height recorded. The percentage reduction in MN height was then reported. All tests were carried out at ambient conditions of 22±2°C and a relative humidity of 43±20%.

Delivery of Theophylline Across Neonatal Porcine Skin

Diffusion of theophylline, a model small (MW 180.17 Da) water-soluble drug with poor passive skin permeation, from polymeric MN arrays and a polymeric patch (same formulation composition, drug loading and preparation conditions as MN arrays) across neonatal porcine skin was investigated *in vitro* using modified Franz diffusion cells (FDC-400 flat flange, 15 mm orifice diameter, mounted on an FDCD diffusion drive console providing synchronous stirring at 600 rpm and thermostated at 37±1°C, Crown Glass Co. Inc., Sommerville, N.J., USA). Theophylline, at a loading of 1% w/w, was included in gels used to prepare MN arrays optimised on the basis of mechanical and insertion tests.

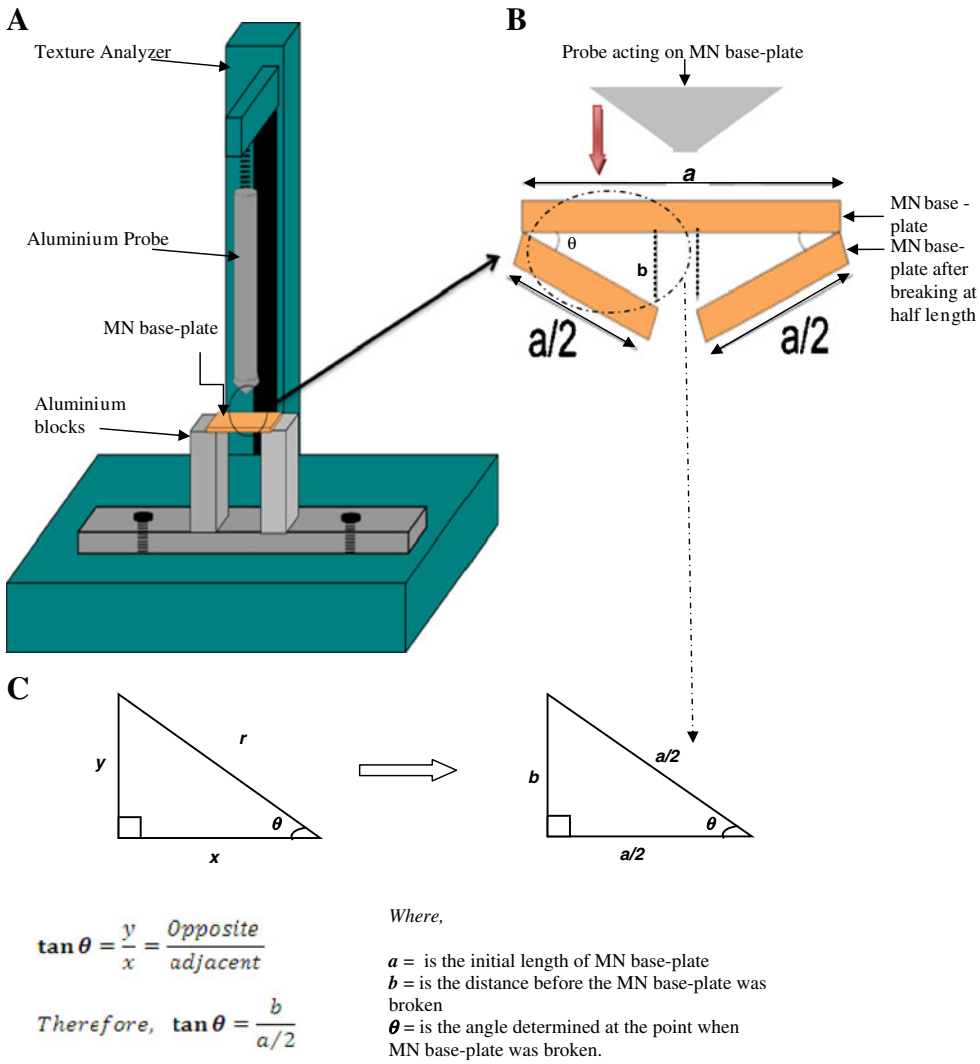

Fig. 4 Illustration of (**A**) the Texture Analyzer set-up; (**B**) the method employed in measuring the degree of flexibility of MN base-plates and (**C**) the equation used to determine the degree of flexibility of MN base-plates.

Neonatal porcine skin samples, obtained as described above, were shaved carefully so as not to damage the skin (31) and pre-equilibrated in phosphate-buffered saline pH 7.4 (PBS) for one hour before beginning the experiments. A circular specimen of the skin was secured to the donor compartment of the diffusion cell using cynoacrylate glue with the *stratum corneum* side facing the donor compartment. Using gentle plunger pressure (approximately 0.1 N per MN, determined using the Texture Analyser in reverse mode), MN were inserted by hand into the centre of the skin, which was supported again underneath by dental wax. The skin was removed from the dental wax and then MN further secured in place using a non-adhesive putty material (BluTac®) on top of the array. With MN arrays in place, donor compartments were mounted onto the receptor compartments of the Franz cells. The receptor medium was PBS, degassed prior to use by sonication. Using a long needle, samples (0.30 ml) were removed from the receptor compartment at defined time intervals and replaced with an equal volume of pre-warmed degassed PBS. Sink conditions were maintained throughout the experiment. The concentrations of theophylline in the receptor medium were determined by HPLC as described below.

Analysis of Theophylline in Solution

Theophylline analysis was performed using HPLC (Agilent 1200® Binary Pump, Agilent 1200®, Standard Autosampler, Agilent 1200® Variable Wavelength Detector, Agilent Technologies UK Ltd., Stockport, UK) with UV detection at 272 nm (32). Separation was done on a Spherisorb® C_{18} column (150 mm×4.5 mm with 5 μm packing, Waters Corporation, Milford, Massachusetts, USA). The injection volume was 100.0 μl, and the mobile phase was 84.0% 10 mM ammonium acetate buffer/8% methanol/8% acetonitrile, v/v/v. The flow rate was 1 ml min^{-1}. Least squares linear regression analysis and correlation analysis were performed on the calibration curve produced,

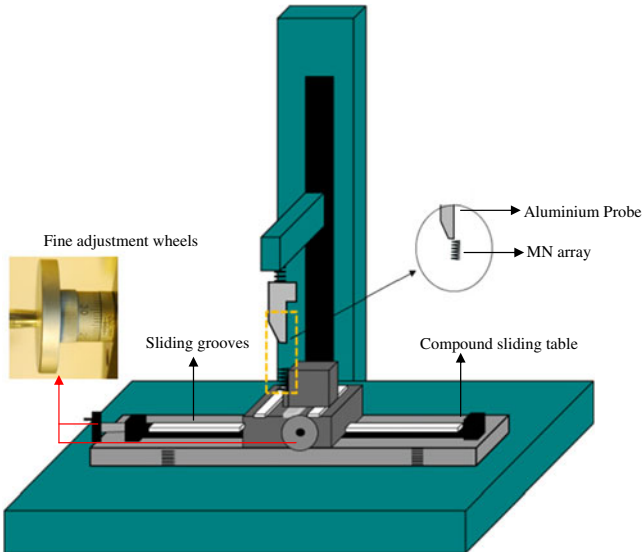

Fig. 5 Illustration of the Texture Analyzer set-up for determination of the bending fracture forces of MN arrays.

enabling determination of the equation of the line, its coefficient of determination and the residual sum of squares (R*SS*). This representative calibration curve was used to determine the limits of detection (*LOD*) and quantification (*LOQ*) of the method. The *LOD* of a chromatographic method may be determined as follows, using Equation 2:

$$LoD = \frac{3.3\sigma}{S} \tag{2}$$

where σ is the standard deviation of the response (peak area) of the data used to construct the regression line and S is the slope of that line. Similarly, the LoQ may be determined using Equation 3:

$$LoQ = \frac{10\sigma}{S} \tag{3}$$

Optical Coherence Tomography

Following local ethical committee approval and fully informed consent, optical coherence tomography (OCT) was used to visualise MN insertion into human skin *in vivo* in 2D and 3D. Optimised drug-free MN arrays were inserted into

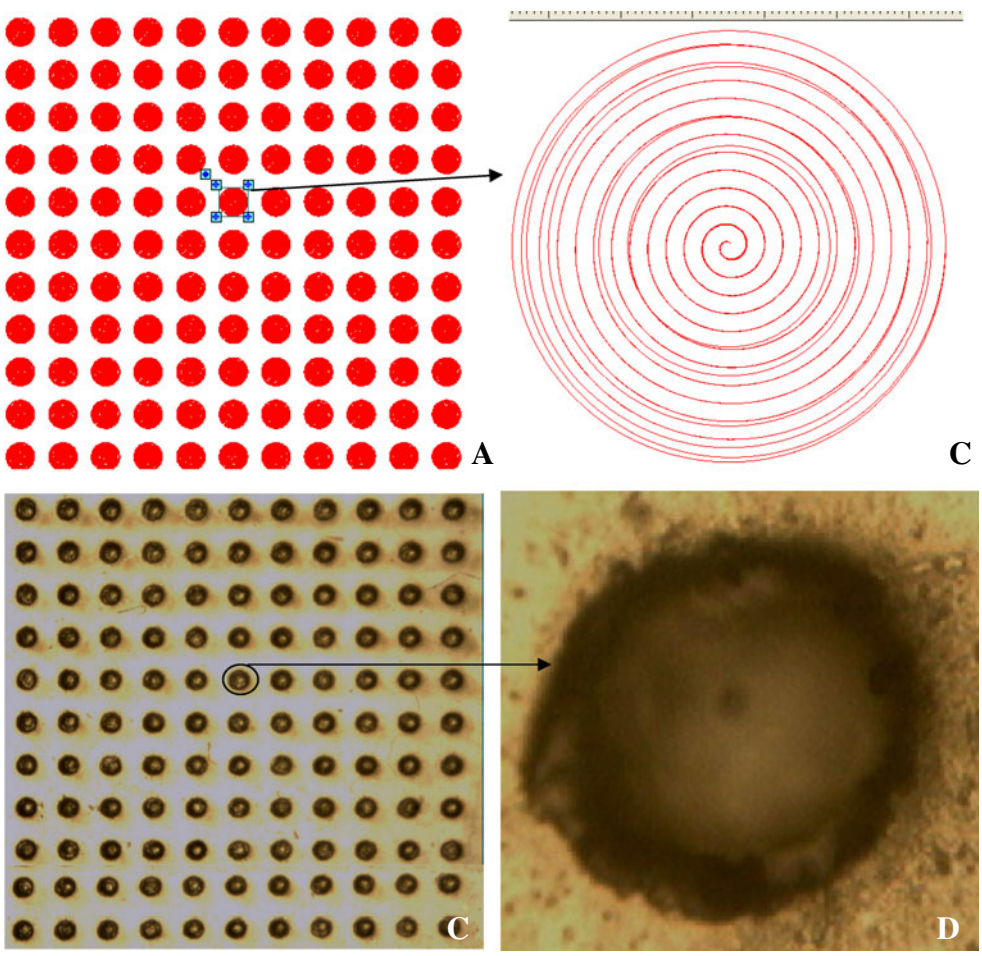

Fig. 6 **A** MN array (11 × 11) pattern drawn on the system for laser engineering of holes into silicone sheets. **B** Strategic image of a single hole. **C** Digital microscope image of laser-engineered silicone micromould (11 × 11) on 1.0 mm thick silicone sheet. (**D**) Digital microscope image of a single hole.

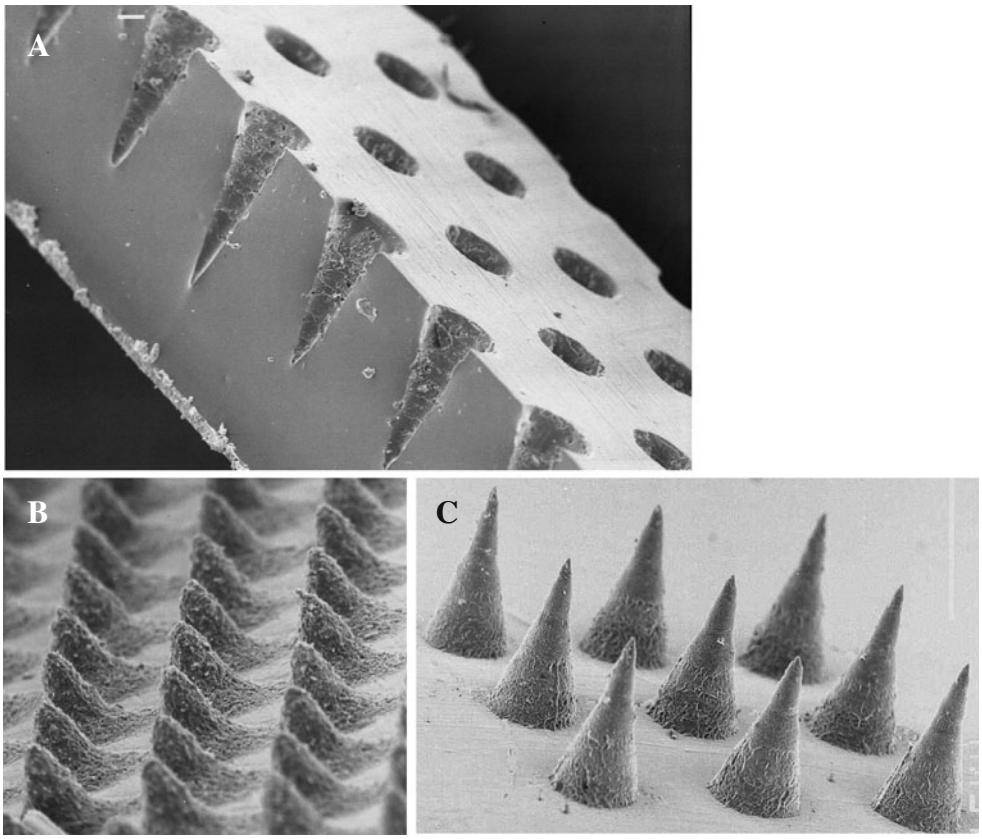

Fig. 7 **A** SEM of the cross-section of a silicone micromould after laser engineering, revealing cone-shaped holes. **B** MN arrays prepared from aqueous blends containing 20% w/w Gantrez® AN 139 with 50 μm height showing roughened outer surface. **C** MN arrays prepared from aqueous blends containing 20% w/w Gantrez® AN 139 with 300 μm height showing optimised surface characteristics.

the forearm of human volunteers using gentle finger pressure. Images were then obtained using a VivoSight® high-resolution OCT Scanner with handheld probe (Michelson Diagnostics Ltd., Kent, UK). The swept-source Fourier domain OCT system has a laser centre wavelength of 1,305 ± 15 nm, facilitating real time high resolution imaging of the upper skin layers (7.5 μm lateral and 10 μm vertical resolution). The skin was scanned at a frame rate of up to 15 B-scans (2D cross-sectional scans) per second (scan width = 2 mm). 2D images were converted into a 3D representation using the imaging software ImageJ® (33). The scale of the image files obtained was 1.0 pixel = 4 μm, thus allowing accurate measurements to be made. To allow differentiation between MN and skin and different skin layers, false colours were applied to OCT images using Ability Photopaint® Version 4.14 (Ability Plus Software Ltd., Crawley, UK).

Statistical Analysis

Where appropriate, data was analysed using a one-way analysis of variance (ANOVA). Mathematical characterisation of the relationships between the x and y variables in the representative calibration plots was performed using least squares linear regression, following analysis of residuals. In all cases, $p < 0.05$ denoted significance.

RESULTS

Fig. 6 shows a screenshot of the machine strategy for an array of needles (11 × 11 array, base diameter of 600 μm, height of 600 μm and interspacing of 300 μm) (A), as well as a close-up of a single needle-shaped hole (B). Digital

Table I Physical Characteristics of Polymeric MN Arrays Produced Using Laser-Engineered Micromoulds

Material	Height (μm)	Width (μm)	Interspacing of MN at base (μm)	Interspacing of MN at tip (μm)	Aspect ratio
PVA	583.68 ± 9.59	285.30 ± 7.09	295.38 ± 9.17	575.16 ± 11.23	2.05
Alginic Acid	517.51 ± 8.35	273.77 ± 9.92	274.91 ± 4.20	546.29 ± 9.33	1.89
Carbopol® 971-P NF	594.96 ± 9.03	293.86 ± 8.67	303.66 ± 5.57	608.79 ± 9.58	2.02
Gantrez® AN 139	608.93 ± 20.08	313.42 ± 10.81	328.57 ± 12.98	679.50 ± 6.32	1.94

(Mean ± SD, $n = 45$)

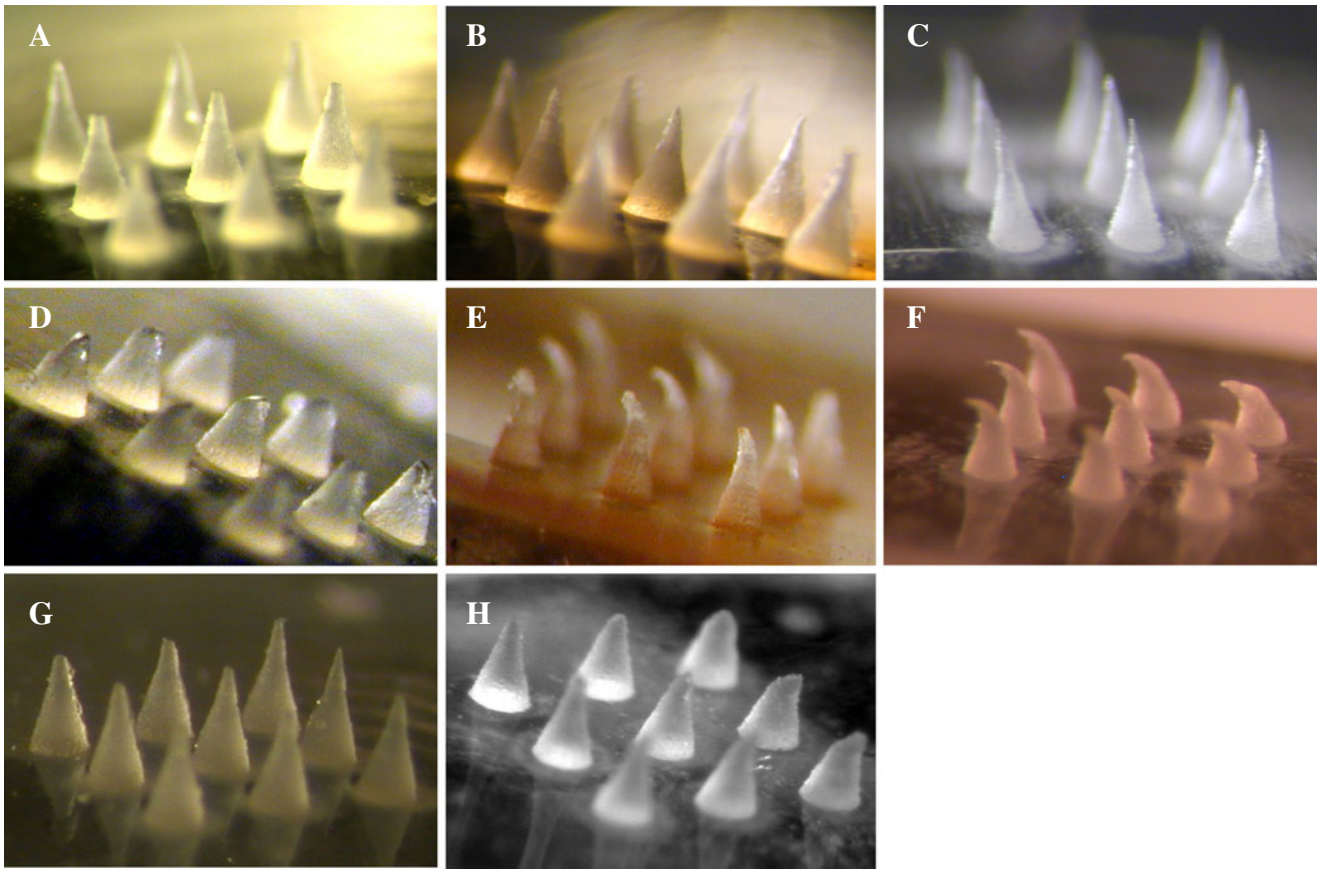

Fig. 8 Light microscope images of polymeric microneedles prepared from aqueous blends containing Carbopol® 971-P NF, alginic acid, poly(vinyl) alcohol and Gantrez® AN-139 before, (**A**, **B**, **C** and **G** respectively), and after (**D**, **E**, **F** and **H**, respectively) the application of a compression force.

microscope (GXMGE-5 digital microscope, Laboratory Analysis Ltd., Devon, England, UK) images of a MN micromould (11×11 array, base diameter of 600 μm, height of 600 μm and interspacing of 300 μm) as well as a single MN mould are also shown in Fig. 6 (C and D).

To facilitate observation of the shape of the holes machined by the laser into the transparent silicone sheets, scanning electron microscope (JEOL JSM840, Tokyo, Japan) images of cross-sectioned moulds were produced, as shown in Fig. 7A. Initial testing produced MN arrays with roughened surfaces (Fig. 7B). As the laser beam is scanned in a given direction, successive pulses overlap each other. The percentage of overlap is determined by the scan speed of the galvanometer and the repetition rate of the laser. Roughness can occur due to a low percentage overlap of the laser beam. To ensure a smoother surface, the percentage overlap of successive laser pulses was optimized at 95%, which produced MN as shown (Fig. 7C). The time taken to machine an array of 11×11 needles with 300 μm width at base, 600 μm height and 300 μm interspacing was approximately 5.4 min. Cleaning the entire micromould down to the tip of each MN indentation was found to be a crucial step in preparation of uniform, consistent, MN arrays.

Utilising the laser-machined MN micromoulds (theoretical dimensions: 600 μm height, 300 μm width at base, and 300 μm interspacing between the base of MN), a range of polymeric formulations was investigated for their potential use in MN fabrication. Whilst all formulations proved capable of production of structurally intact MN arrays (Table I and Fig. 8), there are some points worthy of consideration. In particular, the array formed from a 30%

Table II Influence of Compression Force (0.36 N/needle) on the Physical Dimensions of Polymeric MN

PVA	% Reduction in height of MN		
	Alginic acid	Carbopol® 971-P NF	Gantrez® AN-139
38.73 ± 2.21	42.07 ± 0.89	38.31 ± 3.10	19.54 ± 2.89

(Mean ± SD, $n = 45$)

Table III Theoretical Geometries of Gantrez® AN 139 MN Arrays Produced Using Laser-engineered Micromoulds

Model no	Height (μm)	Base diameter (μm)	Interspacing of MN at base (μm)
1	600	300	300
2	600	300	600
3	600	300	150
4	600	300	50
5	600	300	25
6	300	300	300
7	900	300	300

w/w PVA solution had an irregular-shaped base-plate, with quite a degree of flexibility to its structure. As such, it is doubtful that this formulation would possess the necessary mechanical strength to sufficiently disrupt the *stratum corneum* barrier of the skin. This degree of flexibility was also evident in the arrays formed from aqueous solutions of alginic acid, as well as those produced from Carbopol® 971-P NF. However, it was found that MN arrays formed from aqueous blends of 20% w/w Gantrez® AN-139 possessed a rigid, inflexible structure. These observations are evident in the results obtained following the application of a compression force to the MN arrays (Table II). It was found that the Gantrez® AN-139 MN possessed the greatest ability to resist compression, with only an approximate 20% reduction in the height of the MN occurring following application of a 0.36 N per needle force. This was significantly less than the approximate 40% reduction in height of MN produced from PVA, alginic acid and Carbopol® 971-P NF (in all cases p values <0.05). Digital microscope images of polymeric MN before and after compression testing are shown in Fig. 8. As a result of their poor performance in this preliminary test, MN prepared from PVA, alginic acid and Carbopol® 971-P NF were not evaluated further. Aqueous blends containing 20% Gantrez® AN-139 were used in MN production for the remainder of the study.

Seven different array geometries were prepared. Micromoulds were found to be capable of re-use >100 times, while still producing MN of consistent geometry. Theoretical array parameters (Table III) were generally in good agreement with those produced experimentally (Table IV). These MN were then fully characterised in terms of their mechanical properties. Fig. 9A shows the effect of increasing compression force. MN failure was not observed, even at the maximum force per needle (0.711 N per needle) applied. However, height reduction increased progressively with increasing compression force. As is evident from the results in Fig. 9A, at compression forces of 0.09 N/needle or higher, initial MN height had no significant effect on % reduction in height of MN arrays. At lower compression forces, there was a slight difference in % reduction in height with different initial MN heights. Microscopic inspection (Fig. 10i (A)) showed that compression of the microneedles starts from the tapered tip and proceeds down the shaft base, but all of the MN arrays maintained their out-of-plane structure, with no cracks observed at the base. MN array geometry had little discernable effect on the extent of compression observed, regardless of the force applied.

As can be seen from Table V, once the insertion force was 0.03 N per MN or greater, the majority of MN in an array penetrated the *stratum corneum* of neonate porcine skin *in vitro*, as evidenced by methylene blue staining following MN removal (Fig. 10ii). The exception was model 6, where there was no evidence to suggest that these MN penetrated the *stratum corneum*. Fig. 9B shows that increasing insertion force led to progressive reduction in MN height. The

Table IV Physical Characteristics of MN Arrays Prepared from Aqueous Blends Containing 20% w/w Gantrez® AN 139 Using Laser-Engineered Micromoulds

Model no	Height (μm)	Base diameter (μm)	Interspacing of MN at base (μm)	Interspacing of MN at tips (μm)	Aspect ratio
1	608.93 ± 20.08	313.42 ± 10.81	328.57 ± 12.98	679.50 ± 6.32	1.94
2	649.92 ± 34.95	295.42 ± 15.00	601.05 ± 9.91	938.42 ± 12.15	2.20
3	629.60 ± 43.11	285.73 ± 18.66	162.73 ± 13.55	496.98 ± 8.12	2.20
4	547.52 ± 6.94	292.28 ± 10.44	53.17 ± 2.92	378.73 ± 5.10	1.87
5	613.56 ± 43.58	302.38 ± 15.52	26.37 ± 1.59	342.96 ± 4.82	2.03
6	366.48 ± 21.60	304.19 ± 29.61	323.32 ± 10.60	652.67 ± 14.08	1.20
7	906.82 ± 68.93	337.04 ± 24.39	287.72 ± 19.74	669.38 ± 11.67	2.69

(Means ± SD, $n > 84$)

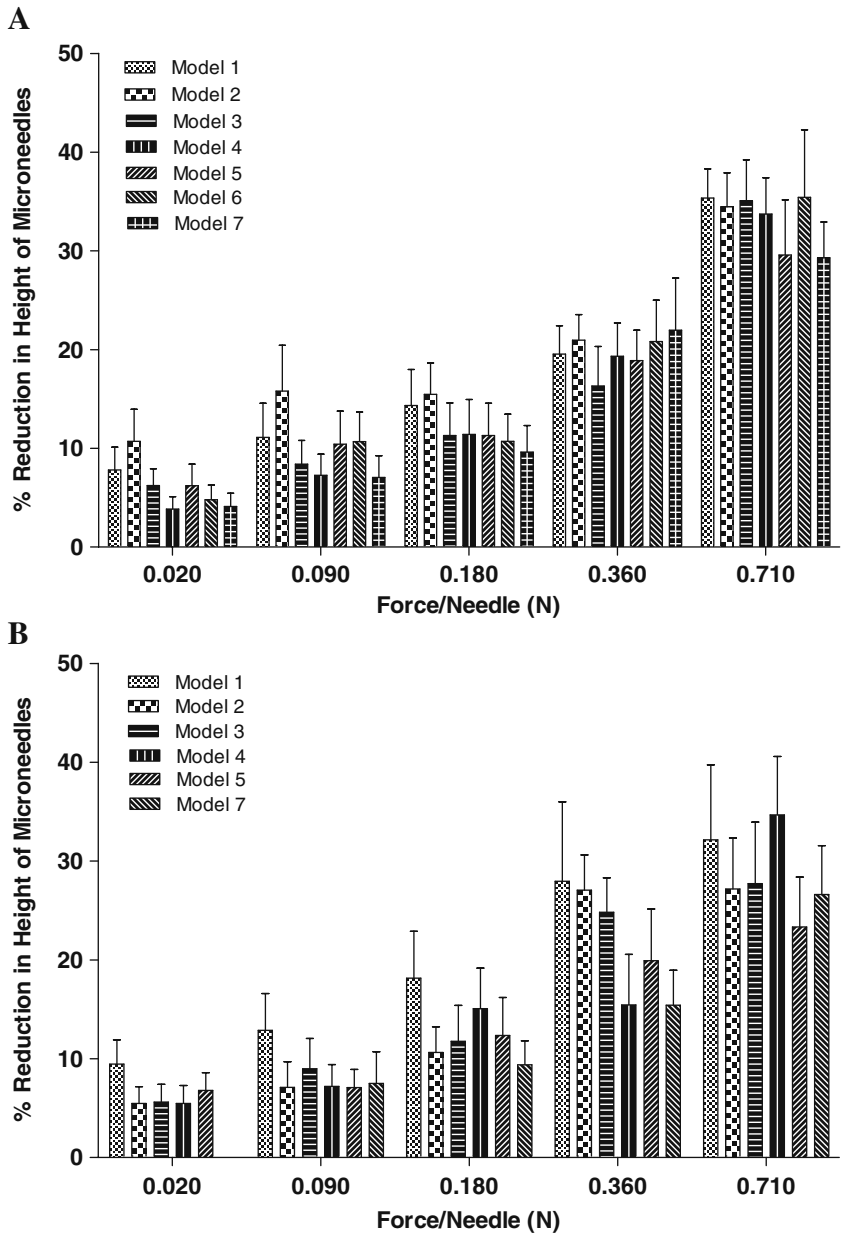

Fig. 9 **A** Percentage reduction in height of MN arrays prepared from aqueous blends containing 20% w/w Gantrez® AN 139 as a function of compression force applied. Means (±SD), $n > 20$. **B** Percentage reduction in height of MN arrays prepared from aqueous blends containing 20% w/w Gantrez® AN 139 as a function of insertion forces applied. Means (± SD), $n > 20$.

relatively high standard deviations observed are likely due in part to initiation of MN dissolution during the 30 s insertion test in skin interstitial fluid (Fig. 10iii). It is also evident from Fig. 9B that, with increase in MN height from 600 µm (Model 1) to 900 µm (Model 7), % reduction in height of MN arrays decreased significantly. This could be due to partial dissolution of MN arrays, which was predictably higher (in terms of % reduction height) for the shorter MN. No height reduction was evident for model 6 MN, regardless of the force of insertion employed, possibly due to no insertion into skin. It is also evident from Fig. 9A and B that interspacing at tips did not significantly affect % reduction in heights of MN arrays.

In order to predict robustness of the material, the break strength and the degree of flexibility of the MN base-plates were evaluated. If the base-plate is too rigid, it may break during insertion, due to the irregular topography of the skin surface on a microscopic scale and the macroscopic curvature of different body regions. Accordingly, the base-plate should ideally possess some degree of flexibility, as well as sufficient strength to withstand handling and insertion. The degree of bending of the base-plate without breaking provides an evaluation of MN substrate flexibility. Base-bending experiments on Gantrez® AN-139 base-plates showed that the force required to break the base-plate was 2.38±0.54 N, with an angle of bending at break of 1.28±0.21°.

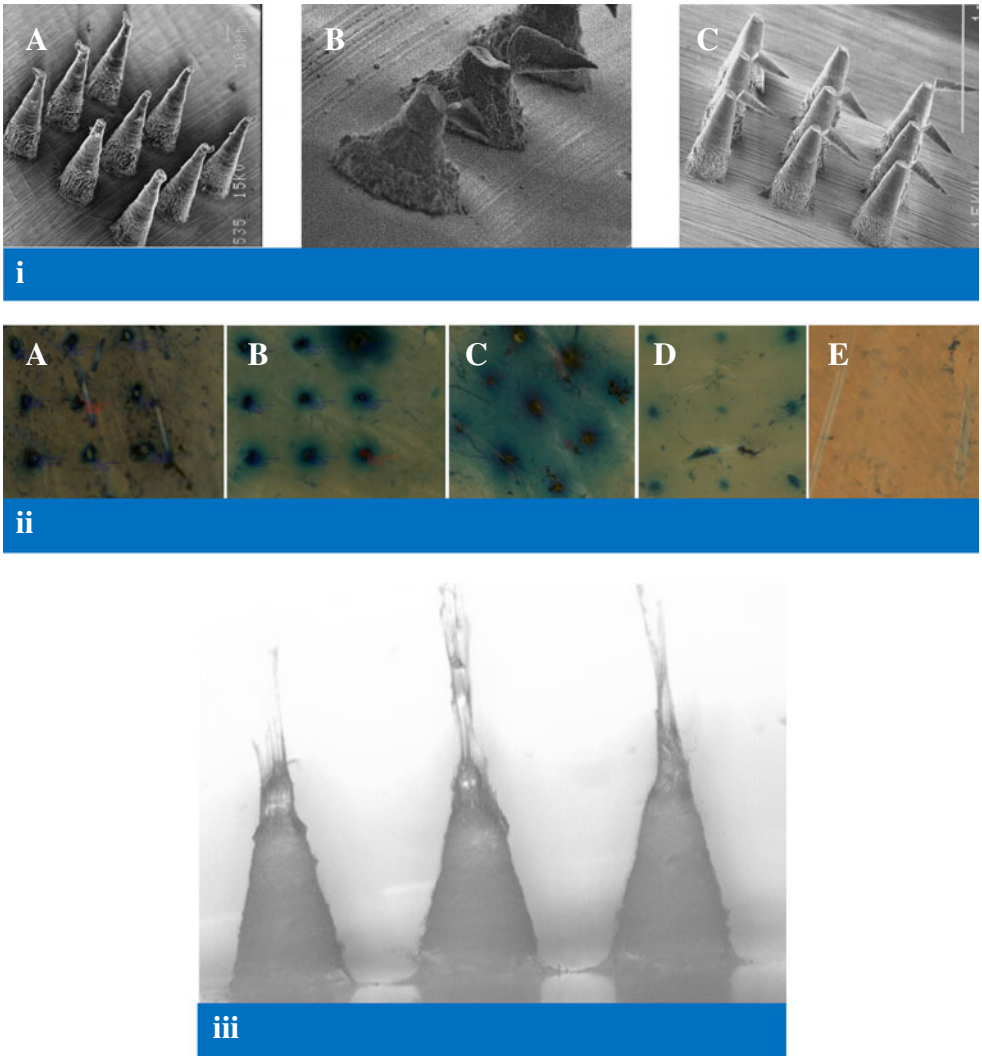

Fig. 10 (i) Scanning electron micrographs of model 7 MN following application of a compression force of 0.02 N per needle (**A**), model 6 MN following application of a force of approximately 0.17 N perpendicular to the MN shaft (**B**), model 1 MN following application of a force of approximately 0.08 N perpendicular to the MN shaft (**C**) (ii) Illustrative digital images of holes created in neonatal porcine skin using various insertion forces for Model 1 MN arrays. A: 0.44 N per needle, B: 0.11 N per needle, C: 0.03 N per needle, D: 0.01 N per needle, E: 0.0056 N per needle. (iii) Illustrative digital image of Gantrez® AN-139 MN arrays (model 3) showing slight elongation in MN tips (due to initiation of dissolution in interstitial tissue fluid) following insertion into neonatal porcine skin for 30 s.

Fig. 10i (C) shows that application of a force (perpendicular to the MN shaft) of approximately 0.08 N per MN (Table VI) caused transverse failure of MN 600 μm in height (model 1), such that the MN height was reduced by approximately 38%. Results were similar for model 7, where the MN were approximately 900 μm in height. However, for model 6, where the MN were originally approximately 300 μm in height, a force of approximately 0.17 N was required to induce transverse failure of the MN shaft, which was then reduced to approximately 50% of its original height (Table VI, Fig. 10i B). Significantly, the forces required to induce transverse failure of MN were greater than the 0.03 N required to allow skin insertion of the majority of MN in an array (Table V).

Due to the substantial reduction in height of 300 μm MN during transverse failure tests and their poor

Table V Percentage of Holes Created in Neonatal Porcine Skin *In Vitro* Following Insertion Tests on MN Arrays Prepared from Aqueous Blends Containing 20% w/w Gantrez® AN 139

Force per MN (N)	Model						
	1	2	3	4	5	6	7
0.03	86.67 ± 18.26	100.00	95.56 ± 6.09	100.00	95.00 ± 6.85	0.00	100.00
0.11	97.78 ± 4.97	100.00	100.00	100.00	97.50 ± 5.59	0.00	100.00
0.44	100.00	100.00	100.00	100.00	98.75 ± 2.80	0.00	100.00

(Means ± SD, $n > 20$)

Table VI Influence of MN Geometry on Force Required to Induce Transverse Failure of MN Prepared from Aqueous Blends Containing 20% w/w Gantrez® AN 139

Model	Force/Needle (N)	% Reduction in Height of MN arrays
1	0.08 ± 0.03	37.48 ± 2.90
6	0.17 ± 0.10	50.43 ± 3.39
7	0.09 ± 0.02	33.38 ± 8.01

(Means ± SD, $n = 36$)

penetration into skin, it was decided that they should not be used for drug delivery studies. Although MN 900 μm in height gave adequate penetration and possessed good physical strength, preliminary *in vivo* human studies revealed that they caused discomfort upon insertion (results not shown). Consequently, 600 μm MN were used for drug delivery and *in vivo* studies.

As there were no statistically significant differences in % reductions in height during compression and insertion tests and in skin penetration results for the various 600 μm MN geometries evaluated, model 1 was arbitrarily chosen and theophylline dissolved into the aqueous Gantrez® blend at a loading of 1% w/w. Increasing drug loading above 1% w/w led to highly flexible materials, unsuitable for MN production, possibly due to placticising action of theophylline on the copolymer. Theophylline-loaded MN had mean heights of 596 μm, mean widths at base of 297 μm, mean interspacing at base of 299 μm and mean interspacing at tips of 602 μm ($n = 45$). The percentage reduction in MN height for a compression force of 0.36 N/needle was approximately 19.47%. In each case, dimensions and percentage reduction in height were not significantly different from unloaded Gantrez® MN ($p > 0.05$ in each case).

Table VII shows the calibration curve properties for the theophylline analytical method. The retention time of theophylline was approximately 5.5 min. The HPLC calibration curve was found to be linear in the range of 100–10,000 ng ml^{-1}. The method was validated for inter- and intraday accuracy and precision (Table VIII), whereby results demonstrated good precision and accuracy. This analytical method was found to be selective, with no interference observed at the retention time of theophylline from Gantrez® AN-139. Stability of theophylline was found to be excellent, with no evidence of degradation for 48 h in the autosampler and 30 days storage under refrigerated conditions (2–8°C).

Fig. 11 compares the *in vitro* permeation profiles of theophylline released from a Gantrez® AN-139 patch and a Gantrez® AN-139 MN array containing the same drug loading across neonatal porcine skin. It is clear from the results that the MN array delivered significantly more drug across the skin compared to the control patch over a period of 24 h. The patch delivered only approximately 5.5% of its total loading across the skin. In contrast, the MN array delivered approximately 83% of its total loading over the same period. With the patch, theophylline permeation was not detectable for the first 4 h of the experiment, whereas with the MN array, theophylline was detectable in the receptor compartment within 5 min.

Fig. 12(A and B) shows cross-sectional images of a 600 μm drug-free Gantrez® AN-139 MN array inserted into human skin *in vivo*. The images confirm that the MN punctured the *stratum corneum* barrier and that the MN extended approximately 460 μm into the skin. The widths of the MN-induced holes in the *stratum corneum* were approximately 265 μm in diameter. However, it is obvious that there was a clear space of approximately 136 μm between the bottom of the MN base-plate and the upper surface of the *stratum corneum*, indicating that the entirety of the MN lengths were not inserted into the skin.

DISCUSSION

Since their first description in 2003 (12), many research groups have carried out extensive work on microneedles (MN) prepared from polymeric materials. There are major advantages of such materials over the metals and silicon traditionally used in MN manufacture. These include the possibility of loading a drug to be delivered into the MN matrix for release in skin by biodegradation or dissolution in skin interstitial fluid and, in many cases, their biocompatibility and biodegradability. A wide variety of polymeric materials have been used in the fabrication of MN, including poly (methylmethacrylate) (PMMA), poly-L-lactic acid (PLA), poly-glycolic acid (PGA), and poly-lactic-co-glycolic acid (PLGA), cyclic-olefin copolymer, poly(vinyl pyrrolidone) and sodium carboxymethylcellulose (4,13,34–40). Most recently, Lee *et al.* (28) described fabrication of MN arrays from aqueous blends of carboxymethylcellulose and amylopectin, rather than molten polymers. The absence of a heating step proved to be a notable advantage in preserving stability of incorporated drug.

Table VII Calibration Curve Properties as Determined by Linear Regression and Correlation Analyses and Limits of Detection and Quantification of Theophylline ($n = 5$)

Slope	y-intercept	r^2	Rss	*LOD* ($ngml^{-1}$)	*LOQ* ($ngml^{-1}$)
269.17	8463.1	0.9999	3.28×10^9	12.68	42.28

Table VIII Accuracy and Precision of the HPLC Method ($n = 5$)

Selected concentration (ngml^{-1})	Mean concentration found (ngml^{-1})	S.D.	C.V. (%)	Accuracy (%)
Inter-day				
300	293.68	13.12	4.46	97.89
4,000	4022.6	59.78	1.49	100.6
8,000	7730.08	315.55	4.08	96.63
Intra-day				
300	297.72	21.64	4.09	96.17
4,000	4023.92	160.10	3.98	100.6
8,000	8177.762	262.41	3.21	102.22

Polymeric MN have been made by a variety of mould-based techniques, including casting (37), hot embossing (35), injection moulding (38), investment moulding (40) and micromoulding (28). Laser-based surface alteration of, and hole creation in, PLA MN previously micromoulded from silicon master MN has been described (34). However, the present study constitutes the first description of polymeric MN prepared at ambient temperatures from aqueous polymer blends by micromoulding using laser-engineered moulds.

Laser micromachining is an ideal technology for use in medical device manufacture. By choosing the appropriate wavelength and pulse width, the ablation process can be either material selective, in that one material will be ablated faster than another material, or non-material selective, in that all material will be machined at a similar rate. The laser process is inherently non-contact, which allows it to be used in the dust-free and sterile environments necessary for medical device manufacture. Finally, the running costs of laser units, in particular diode-pumped solid-state (DPPS) lasers, are relatively low.

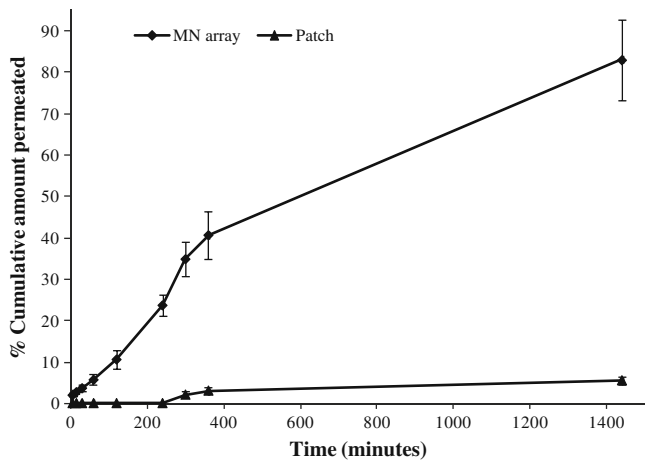

Fig. 11 Comparative permeation profiles of theophylline across neonatal porcine skin when released from a Gantrez® AN-139 patch and a Gantrez® AN-139 MN array containing the same drug loading. Means (± SD), $n > 3$.

Traditional methods of laser micromachining, such as 248 nm excimer-based mask projection techniques (34), allow the creation of precise shapes in polymer materials. However, the time to prototype is limited by the creation of masks, and all but the simplest of shapes, such as holes or squares, cannot be manufactured in a timely manner. As a scalable production process, the use of mask technology is well proven (41). However, the cost of consumables, such as masks and gas refills, make excimer-based processing a high-cost option.

Replacing mask projection-based beam delivery with galvanometer-based beam delivery is fast becoming the standard method of high throughput, low cost laser micromachining. Galvanometer-based laser micromachining allows the position and on/off pulsing of the laser beam to be determined by a standard computer-aided design (CAD) file. The galvanometer consists of two mirrors that can position the beam to either a given point within a field of view or, more importantly, scan the laser beam within the field of view. Therefore, the laser beam can trace out a CAD-based design onto the work piece, without the need for masks. This makes it ideal for fast prototyping and is scalable to production volume runs. The lack of consumables, such as masks, also makes it a cheaper option.

In the present study, a galvanometer-based laser micromachining method was employed to engineer silicone micromoulds, allowing MN to be prepared from aqueous polymeric blends. Simple alteration of this method allowed MN with relatively smooth surfaces to be produced. Of the widely used pharma polymers investigated here, Gantrez® AN-139, normally used as a mucoadhesive in denture fixatives, was surprisingly found to produce MN with the greatest resistance to mechanical deformation. This is likely to be important, because, as the field moves forward, polymeric microneedle arrays intended for drug/vaccine delivery purposes should be suitably robust to withstand handling by patients and/or clinicians prior to insertion and be of sufficient rigidity to enable skin penetration. Of the seven different MN geometries prepared from aqueous blends containing 20% w/w Gantrez® AN-139, only MN with heights of 300 μm failed to penetrate neonate porcine

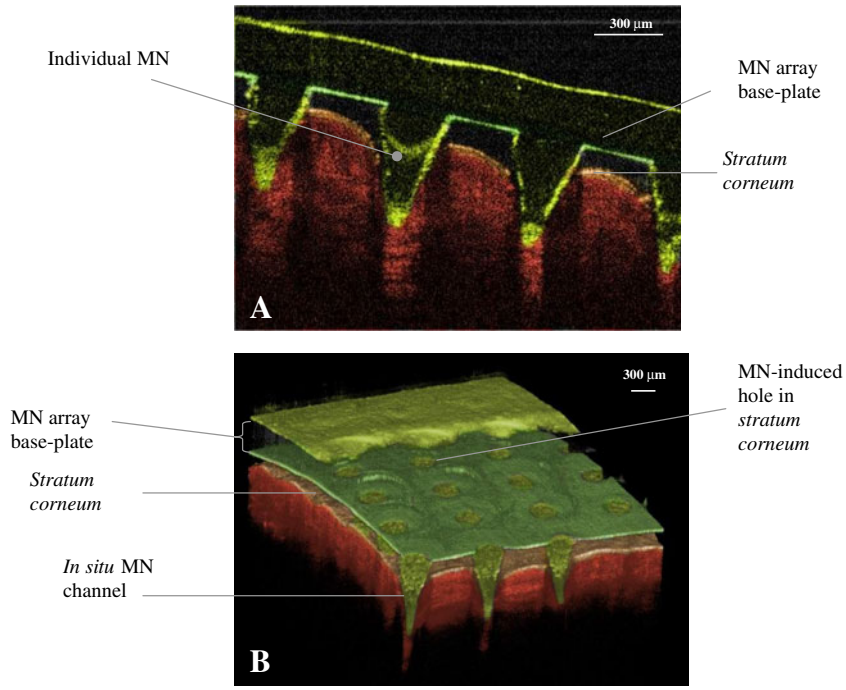

Fig. 12 OCT images showing MN (height 600 μm, width at base 300 μm, spacing 300 μm) inserted into human skin *in vivo* in 2D (**A**) and 3D (**B**).

skin upon application of forces of 0.03 N/needle and greater. All MN were relatively resistant to transverse failure, and MN base-plates demonstrated good mechanical strength and reasonable flexibility.

Incorporation of the model water-soluble drug theophylline above loadings of 1% w/w caused softening of the Gantrez® AN-139 MN materials upon moulding. This is unsurprising given the effects of incorporated drugs on MN strength reported by other workers (24). However, MN micromoulded from aqueous blends containing 20% w/w Gantrez® AN-139 and 1% w/w theophylline possessed mechanical properties not significantly different from their non-drug-loaded counterparts. Use of such systems greatly enhanced transdermal delivery of theophylline *in vitro*.

Optimised Gantrez® AN-139 MN arrays were shown using optical coherence tomography (OCT) to not only puncture the *stratum corneum* of human skin *in vivo*, but also to protrude quite deeply into the underlying viable epidermis and upper dermis. OCT is a non-invasive imaging technique based on light reflection and has been used for a number of medical applications, including imaging of the retina and diagnosis of neoplastic skin lesions (42,43). In this study, OCT was used to visualise polymeric MN arrays in real time whilst inserted into human skin *in vivo*. To date, MN puncture has been confirmed either by applying a coloured dye to the surface of the skin (44) or by measuring transepithelial water loss following MN removal (45). Although these techniques confirm whether the *stratum corneum* has been compromised, they provide no information with regards to the true depth of MN penetration. In this case, the MN penetrated skin to a depth of approximately 77% of the MN shaft length, leaving a clear gap between *stratum corneum* and MN base-plate. Compression of dermal tissue by the inserted MN was here using OCT.

In this study, we have shown, for the first time, the utility of a galvanometer-controlled excimer laser in engineering re-useable micromoulds for production of polymeric MN at ambient temperatures. Importantly, this method enables the fabrication of MN moulds of almost any height and interspacing. Furthermore, laser-machining could also be used to post-process polymeric MN, thus enabling production of hollow or grooved needles. Aqueous blends containing 20% w/w Gantrez® AN-139 proved to be highly suitable for MN fabrication. Such MN were robust, penetrated skin effectively *in vitro* at relatively low insertion forces and greatly enhanced transdermal delivery *in vitro*. However, OCT showed that somewhat less than the entire length of the MN penetrated human skin *in vivo*. While the true significance of this finding is not clear as yet, we are currently carrying out an extensive OCT-informed study investigating the influence of MN array geometry on skin penetration depth, with a view to enhanced transdermal drug delivery from Gantrez® AN-139 MN.

ACKNOWLEDGEMENTS

This work was supported by BBSRC grant number BB/E020534/1 and Invest Northern Ireland Proof of Concept grant number POC21A. The authors thank Dr. Daniel Woods for his assistance with OCT and Michelson

Diagnostics (Kent, England) for the use of their OCT imaging equipment.

REFERENCES

1. Henry S, McAllister DV, Allen MG, Prausnitz MR. Microfabricated microneedles: a novel approach to transdermal drug delivery. J Pharm Sci. 1998;87:922–5.
2. Prausnitz MR. Microneedles for transdermal drug delivery. Adv Drug Deliv Rev. 2004;56:581–7.
3. Davis SP, Martanto W, Allen MG, Prausnitz MR. Hollow metal microneedles for insulin delivery to diabetic rats. IEEE Trans Biomed Eng. 2005;52:909–15.
4. Moon SJ, Lee SS, Lee HS, Kwon TH. Fabrication of microneedle array using LIGA and hot embossing process. Microsyst Technol Micro Nanosyst Informat Storage Proc Syst. 2005;11:311–8.
5. Park JH, Allen MG, Prausnitz MR. Biodegradable polymer microneedles: fabrication, mechanics and transdermal drug delivery. J Control Release. 2005;104:51–66.
6. Stoeber B, Liepmann D. Arrays of hollow out-of-plane microneedles for drug delivery. J Microelectromech Syst. 2005;14:472–9.
7. Trichur R, Kim S, Zhu X, Suk JW, Hong C-C, Choi J-W, *et al.* Development of plastic microneedles for transdermal interfacing using injection molding techniques. Micro Total Analysis System. 2002;1:395–7.
8. Yang M, Zahn JD. Microneedle insertion force reduction using vibratory actuation. Biomed Microdevices. 2004;6:177–82.
9. Donnelly RF, Morrow DIJ, McCarron PA, Woolfson AD, Morrissey A, Juzenas P, *et al.* Microneedle-mediated intradermal delivery of 5-aminolevulinic acid: potential for enhanced topical photodynamic therapy. J Control Release. 2008;129:154–62.
10. Mikszta JA, Dekker JP, Harvey NG, Dean CH, Brittingham JM. Microneedle-based intradermal delivery of the anthrax recombinant protective antigen vaccine. Infect Immun. 2006;74:6806–10.
11. Coulman SA, Barrow D, Anstey A, Gateley C, Morrissey A, Wilke N. Minimally invasive cutaneous delivery of macromolecules and plasmid DNA *via* microneedles. Curr Drug Deliv. 2006;3:65–75.
12. McAllister DV, Wang PM, Davis SP, Park JH, Canatella PJ, Allen MG, *et al.* Microfabricated needles for transdermal delivery of macromolecules and nanoparticles: fabrication methods and transport studies. Proc Natl Acad Sci U S A. 2003;100:13755–60.
13. Gill HS, Prausnitz MR. Coated microneedles for transdermal delivery. J Control Release. 2007;117:227–37.
14. Cormier M, Johnson B, Ameri M, Nyam K, Libiran L, Zhang DD. Transdermal delivery of desmopressin using a coated microneedle array patch system. J Control Release. 2004;97:503–11.
15. Ito Y, Jun-Ichiro Y, Keiji S, Nobuyuki S, Kanji T. Self-dissolving microneedles for the percutaneous absorption of EPO in mice. J Drug Target. 2006;14:255–61.
16. Donnelly RF, Morrow DIJ, McCarron PA, Woolfson AD, Morrissey A, Juzenas P, *et al.* Microneedle arrays permit true intradermal delivery of a preformed photosensitiser. Photochem Photobiol. 2009;85:195–204.
17. Widera G, Johnson J, Kim L, Libiran L, Nyam K, Daddona PE, *et al.* Effect of delivery parameters on immunization to ovalbumin following intracutaneous administration by a coated microneedle array patch system. Vaccine. 2006;24:1653–64.
18. Wang PM, Cornwell M, Hill J, Prausnitz MR. Precise microinjection into skin using hollow microneedles. J Invest Dermatol. 2006;126:1080–7.
19. Ito Y, Eiji H, Atsushi S, Nobuyuki S, Kanji T. Feasibility of microneedles for percutaneous absorption of insulin. Eur J Pharm Sci. 2006;29:82–8.
20. Kaushik S, Allen HH, Donald DD, McAllister DV, Smitra S, Allen MG, *et al.* Lack of pain associated with microfabricated microneedles. Anesth Analg. 2001;92:502–4.
21. Donnelly RF, Thakur RRS, Tunney MM, Morrow DIJ, McCarron PA, O'Mahony C, *et al.* Movement of microorganisms through microneedle-induced holes *is* possible, but initiation of infection is unlikely. Pharm Res. 2009;26:2513–22.
22. Banga AK. Microporation applications for enhancing drug delivery. Expert Opin Drug Deliv. 2009;6:343–54.
23. Martanto W, Davis SP, Nicholas RH, Wang J, Gill HS, Prausnitz MR. Transdermal delivery of insulin using microneedles *in vivo*. Pharm Res. 2004;21:947–52.
24. Park JH, Allen MG, Prausnitz MR. Polymer microneedles for controlled-release drug delivery. Pharm Res. 2006;23:1008–19.
25. Donnelly RF, Morrow DIJ, Thakur RRS, Migalska K, McCarron PA, O'Mahony C, *et al.* Processing difficulties and instability of carbohydrate microneedle arrays. Drug Devel Ind Pharm. 2009;35:1242–54.
26. Kalluri H, Banga A. Kinetics of pore closure in microneedle treated skin. CRS Denmark, July 2009.
27. Arora A, Prausnitz M, Mitragotri S. Micro-scale devices for transdermal drug delivery. Int J Pharm. 2008;364:227–36.
28. Lee JW, Park JH, Prausnitz MR. Dissolving microneedles for transdermal drug delivery. Biomaterials. 2008;29:2113–24.
29. Woolfson AD, McCafferty DF, McCallion CR, McAdams ET, Anderson J McC. Moisture-activated, electrically conducting bioadhesive hydrogels as interfaces for bioelectrodes: effect of film hydration on cutaneous adherence in wet environments. J Appl Polym Sci. 1995;58:1291–6.
30. Fourtanier A, Berrebi C. Miniature pig as an animal model to study photoaging. Photochem Photobiol. 1989;50:771–84.
31. Colea L, Heard C. Skin permeation enhancement potential of Aloe Vera and a proposed mechanism of action based upon size exclusion and pull effect. Int J Pharm. 2007;333:10–6.
32. Nirogi RVS, Kandikere VN, Shukla M, Mudigonda K, Ajjala DR. A simple and rapid HPLC/UV method for the simultaneous quantification of theophylline and etofylline in human plasma. J Chromatogr B. 2007;848:271–6.
33. Girish V, Vijayalakshmi A. Affordable image analysis using NIH Image/ImageJ. Ind J Cancer. 2004;41:47.
34. Aoyagi S, Hayato I, Yuichi I, Mitsuo F, Ogawa H. Laser fabrication of high aspect ratio thin holes on biodegradable polymer and its application to a microneedle. Sens Actuators A Phys. 2007;139:293–302.
35. Han M, Hyun DH, Park HH, Lee SS, Kim CH, Kim CG. A novel fabrication process for out-of-plane microneedle sheets of biocompatible polymer. J Micromechanics Microengineering. 2007;17:1184–91.
36. Ovsianikov A, Chichkov B, Mente P, Monteiro-riviere NA, Doraiswamy A, Narayan RJ. Two photon polymerization of polymer-ceramic hybrid materials for transdermal drug delivery. Int J Appl Ceramic Technol. 2007;4:22–9.
37. Perennes F, Marmiroli B, Matteucci M, Tormen M, Vaccari L, Fabrizio ED. Sharp beveled tip hollow microneedle arrays fabricated by LIGA and 3D soft lithography with polyvinyl alcohol. J Micromechanics Microengineering. 2006;16:473–9.
38. Sammoura F, Kang JJ, Heo YM, Tae SJ, Liwei L. Polymeric microneedle fabrication using a microinjection molding technique. Microsyst Technol. 2007;13:517–22.
39. Sullivan SP, Murthy N, Prausnitz MR. Minimally invasive protein delivery with rapidly dissolving polymer microneedles. Adv Mater. 2008;20:933–8.
40. Lippmann JM, Geiger EJ, Albert AP. Polymer investment molding: method for fabricating hollow, microscale parts. Sens Actuators A Phys. 2007;134:2–10.
41. Madou MJ. Fundamentals of microfabrication. 2nd ed. Boca Raton: CRC Press; 1997. p. 1–71.

42. Landa G, Rosen RB, Garcia PMT, Seiple WH. Combined three-dimensional spectral OCT/SLO topography and microperimetry: Steps toward achieving functional spectral OCT/SLO. Ophthalmic Res. 2009;43:92–8.
43. König K, Speicher M, Bückle R, Reckfort J, McKenzie G, Welzel J, *et al.* Clinical optical coherence tomography combined with multiphoton tomography of patients with skin diseases. J Biophoton. 2009;2:389–97.
44. Haq MI, Smith E, John DN, Kalavala M, Edwards C, Anstey A, *et al.* Clinical administration of microneedles: skin puncture, pain and sensation. Biomed Microdev. 2009;11:35–47.
45. Pearton M, Allender C, Brain K, Anstey A, Gateley C, Wilke N, *et al.* Gene delivery to the epidermal cells of human skin explants using microfabricated microneedles and hydrogel formulations. Pharm Res. 2007;25:407–16.